Class Allocation for Soft-Then-Hard Subpixel Mapping Algorithms With Adaptive Visiting Order of Classes

Qunming Wang, Wenzhong Shi, and Hua Zhang

***Abstract*—The soft-then-hard subpixel mapping (STHSPM) algorithm is a type of subpixel mapping (SPM) algorithm consisting of soft class value (between 0 and 1) estimation and hard class allocation for each subpixel. This letter presents a new class allocation method for STHSPM algorithm. As an extension of our previous work in which subpixels for classes are decided in units of classes (UOC), the new approach, named adaptive UOC (AUOC), improves UOC with adaptive visiting order of classes. In AUOC, the visiting order of classes within each coarse pixel is determined based on the local structure rather than the global structure in UOC. Experiments on three remote sensing images show that AUOC is able to improve UOC in terms of SPM accuracy, particularly for SPM with small zoom factors.**

***Index Terms*—Class allocation, remote sensing, subpixel mapping (SPM), superresolution mapping.**

I. Introduction

SUBPIXEL mapping (SPM) is the goal of predicting a hard classified land-cover map at a finer spatial resolution than that of the input coarse spatial resolution remote sensing image [1]. SPM is also termed superresolution mapping in remote sensing. It can be considered as a postprocessing step of soft classification by dividing the original coarse resolution mixed pixel into multiple subpixels and predicting their land-cover classes under the constraint that the overall pixel-level land-cover proportions should match those predicted by soft classification. In recent years, SPM has received increasing attention, and many algorithms have been developed. In our previous work [2], two basic types of SPM algorithms were summarized. The first type involves initialization and optimization (such as the pixel-swapping [3], genetic algorithm [4], and particle swarm optimization [5] methods). The second type, which is called the soft-then-hard SPM (STHSPM) algorithm [2], contains two steps, i.e., soft class estimation and class allocation [6]–[11]. SPM can be also realized by a contouring method [12] and a one-stage method that do not rely on soft classification [13]–[15].

In the STHSPM approach, the task of soft class estimation is to predict the probabilities of class occurrence at each subpixel, whereas the task of class allocation is to allocate hard class labels to each subpixel according to the predicted probabilities and the proportion constraint from the soft classification. The soft class estimation can be accomplished by a subpixel/pixel spatial attraction model (SPSAM) [6], Hopfield neural network [7], [8], kriging [9], and indicator cokriging (ICK) [10], [11] among several techniques. Regarding class allocation, an approach has been recently developed in [2] that allocates classes in units of classes (UOC). UOC is processed on the fine spatial resolution probability map of each class in turn and has the unique advantage of taking the intraclass spatial dependence into consideration while allocating classes.

In the UOC-based class allocation method, different visiting orders of classes lead to different SPM results and the order needs to be specified reasonably. As presented in [2], the visiting order of classes can be determined by comparing the intraclass spatial correlation quantified by the Moran index, and the classes with stronger autocorrelation need to be visited first. In [2], the Moran index of each class was calculated using the entire proportion image generated by soft classification, which does not need any prior class information. In this way, however, the visiting order of classes is fixed for each coarse spatial resolution pixel. It is known that the spatial structure of land cover varies from area to area and the spatial autocorrelation of a class is usually not the same in all areas of an image. For example, in a local area of the studied image, the spatial continuity of a certain class may be the greatest among all classes and that class should be visited first for the coarse pixels, but in another area, the Moran index of that same class may be the lowest and the class should be visited last. Therefore, using the Moran index calculated from the entire proportion image, the globally specified visiting order may not be the most suitable for all coarse pixels.

This letter aims to extend UOC with an adaptive scheme. In the proposed class allocation method, called the adaptive UOC (AUOC), the spatial correlation is quantified using the local structure information and AUOC is implemented on a per-coarse pixel basis. The remainder of this letter is organized as follows. In Section II, the STHSPM algorithm and UOC-based class allocation method are briefly introduced, followed by details of the proposed AUOC. Experimental results are provided in Section III. Section IV concludes this letter.

Manuscript received September 8, 2013; revised October 30, 2013 and December 13, 2013; accepted December 23, 2013. Date of publication January 17, 2014; date of current version March 14, 2014. This work was supported in part by the Ministry of Science and Technology of China under Project 2012BAJ15B04 and Project 2012AA12A305 and in part by the National Natural Science Foundation of China under Grant 41201451.

Q. Wang and W. Shi are with the Department of Land Surveying and Geo-Informatics, The Hong Kong Polytechnic University, Kowloon, Hong Kong (e-mail: wqm11111@126.com; lswzshi@polyu.edu.hk).

H. Zhang is with the Key Laboratory for Land Environment and Disaster Monitoring of SBSM, China University of Mining and Technology, Xuzhou 221116, China (e-mail: zhhuamesi@gmail.com).

Color versions of one or more of the figures in this paper are available online at http://ieeexplore.ieee.org.

Digital Object Identifier 10.1109/LGRS.2013.2296628

II. METHODS

Let S be the zoom factor, P_t ($t = 1, 2, \ldots, M$, M is the number of pixels in the coarse spatial resolution image) be a coarse pixel, and p_i ($i = 1, 2, \ldots, MS^2$) be a subpixel. Suppose that $F_k(P_t)$ is the proportion of the kth ($k = 1, 2, \ldots, K$, where K is the number of classes) class in coarse pixel P_t and $F_k(p_i)$ is the soft class value for the kth class at subpixel p_i.

A. Soft Class Value Estimation for STHSPM Algorithm

The first step of the STHSPM algorithm is to estimate the soft class value for each subpixel, which indicates the probability of a subpixel belonging to each class. The algorithms that can be used for this step have been introduced in detail in [2]. From [16] and [17], it can be seen that image interpolation algorithms can also estimate soft class values and can be developed into STHSPM algorithms. In this letter, we focus on five fast STHSPM algorithms, including bilinear interpolation, bicubic interpolation, SPSAM, kriging, and ICK, which are employed to predict $\{F_k(p_i)|i = 1, 2, \ldots, MS^2;\ k = 1, 2, \ldots, K\}$.

B. UOC-Based Class Allocation for the STHSPM Algorithm

The second step of the STHSPM algorithm is class allocation. Based on the UOC method, within a coarse pixel, subpixels for the visited class (e.g., class k) are determined by comparison of soft class values $F_k(p_i)$ of all S^2 subpixels. The subpixels with larger soft values of class k are more likely to be allocated to class k. The number of subpixels for class k within a coarse pixel P_t, denoted as $E_k(P_t)$, is determined as

$$E_k(P_t) = F_k(P_t)S^2. \tag{1}$$

Once a subpixel is allocated to a class, it will not be considered in the class allocation process for the remaining classes. Generally, the classes with greater spatial autocorrelation are desired to be visited before those with weaker autocorrelation. The Moran index is used to quantify the spatial autocorrelation such that a larger index corresponds to greater autocorrelation. The index of class k, denoted as I_k, is calculated using the entire proportion image

$$I_k = \frac{M \sum_{i=1}^{M} \sum_{j=1}^{M} W_{ij} \left[F_k(P_i) - \overline{F_k}\right] \left[F_k(P_j) - \overline{F_k}\right]}{\left(\sum_{i=1}^{M} \sum_{j=1}^{M} W_{ij}\right) \sum_{i=1}^{M} \left[F_k(P_i) - \overline{F_k}\right]^2} \tag{2}$$

where $\overline{F_k}$ is the mean of all M proportions for the kth class in proportion image F_k, and

$$W_{ij} = \begin{cases} 1, & \text{if } P_i \text{ and } P_j \text{ are neighbors} \\ 0, & \text{otherwise.} \end{cases} \tag{3}$$

After all K indices are calculated, they are ranked in a decreasing order and the classes with the larger indices are visited first.

C. AUOC-Based Class Allocation for STHSPM Algorithm

It can be seen from UOC that using the entire class proportion image, the Moran index of each class is computed only once. In this way, a single visiting order is defined for all classes and is applied to determine the class allocation process for every coarse pixel. In the entire coarse image, however, the spatial structure of land cover is always complex and the spatial autocorrelation of a class in the entire studied area cannot be characterized adequately by a fixed Moran index in general. The autocorrelation of a class may be the greatest in some local areas but may also be the weakest in other local areas. Consequently, the single visiting order is unlikely to be universally satisfactory for all coarse pixels. To overcome this shortcoming of the UOC-based class allocation method, the autocorrelation needs to be quantified in a spatially adaptive way and AUOC is proposed for this purpose.

In AUOC, the Moran index is calculated on a per-coarse pixel basis and the visiting order of classes within each coarse pixel is determined according to the spatial autocorrelation in the local area, which is centered at the coarse pixel. More precisely, a local window with a size of N by N pixels is selected for each coarse pixel. Using the Moran index, the spatial autocorrelation of class k in the local area for a coarse pixel (e.g., P_t) is quantified as

$$I_k^t = \frac{N^2 \sum_{i=1}^{N^2} \sum_{j=1}^{N^2} W_{ij} \left[F_k\left(P_i^t\right) - \overline{F_k^t}\right] \left[F_k\left(P_j^t\right) - \overline{F_k^t}\right]}{\left(\sum_{i=1}^{N^2} \sum_{j=1}^{N^2} W_{ij}\right) \sum_{i=1}^{N^2} \left[F_k\left(P_i^t\right) - \overline{F_k^t}\right]^2} \tag{4}$$

where P_i^t and P_j^t denote any coarse pixel in the local window centered at P_t, and $\overline{F_k^t}$ is the mean of all proportions for the kth class in the local window. The visiting order of K classes within P_t is specified by comparing all K indices (i.e., $I_1^t, I_2^t, \ldots, I_K^t$). As done in UOC, the classes with larger indices are given priority in AUOC-based class allocation.

As the local proportion image varies from window to window, the calculated Moran indices for all coarse pixels are different. Hence, in the AUOC method, the specified visiting order of classes is a function of the location of the coarse pixel. This is different from UOC that specifies the visiting order based on a per-global-image basis. The advantages of the proposed AUOC are as follows.

1) Similar to UOC, AUOC also takes the intraclass spatial dependence into account during class allocation process.
2) As shown in (4), AUOC does not need any prior class information to determine the visiting order of classes. This is also the same as UOC.
3) AUOC behaves adaptively and selects the most suitable visiting order of classes within a coarse pixel according to the surrounding pixels.

D. Implementation of AUOC

The implementation of AUOC consists of the following steps.

Step 1: Select a coarse pixel P_t from the coarse spatial resolution image.

Step 2: Find the local window with a size of N by N pixels that is centered at P_t.

Step 3: Calculate the Moran indices of K classes, i.e., $I_1^t, I_2^t, \ldots, I_K^t$, according to (4).

Step 4: Determining the visiting order of classes by comparison of the K indices: $I_1^t, I_2^t, \ldots, I_K^t$.

Step 5: According to the specified visiting order, subpixels for each class are determined class by class. The class

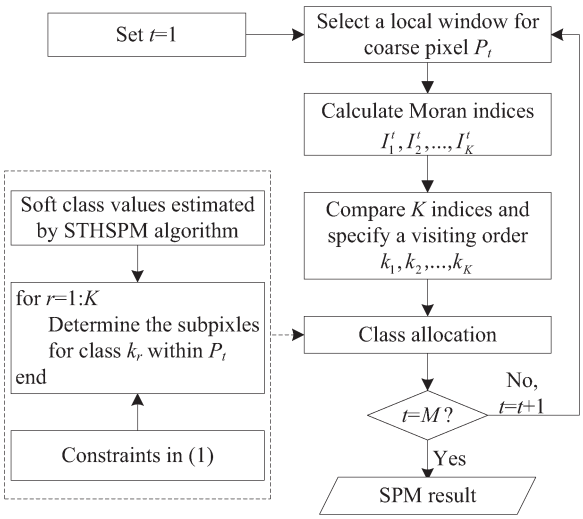

Fig. 1. Flowchart of the proposed AUOC-based class allocation method.

allocation process is implemented with soft class values that have been predicted by the STHSPM algorithm under the constraints presented in (1). Readers may refer to [2] for details.

Step 6: The whole process is terminated when all subpixels within all coarse pixels are allocated to a class. Fig. 1 is the flowchart of the AUOC-based class allocation method.

III. Experiments

Experiments were conducted using three remote sensing images to test the AUOC method. To avoid the uncertainty in soft classification and concentrate only on the performance of SPM, synthetic proportion images were used. Specifically, the original images were classified with a hard classifier to yield land-cover maps. Each land-cover map was decomposed into K binary land-cover maps, and then proportion images were simulated by degrading the binary land-cover maps with an S by S mean filter. SPM was performed to reproduce the fine spatial resolution land-cover map with zoom factor S, and the original fine-resolution map was used for accuracy assessment of SPM. Since SPM is essentially a hard classification technique (but at the subpixel scale), the accuracy of SPM was quantitatively evaluated by the overall accuracy in terms of the percentage of correctly classified pixels (PCC). Note that the nonmixed pixels were not included in the accuracy statistics because they will only increase the PCC without providing any useful information on the performance of SPM [6], [18]. Five STHSPM algorithms were implemented, namely, bilinear interpolation, bicubic interpolation, SPSAM, kriging, and ICK. The proposed AUOC was applied to the five STHSPM algorithms and also compared to UOC for validation.

A. Data

The first image is provided by Hyperspectral Digital Imagery Collection Experiment (HYDICE) airborne hyperspectral data. The data cover an area in Washington, DC Mall (191 bands with a spatial resolution of 3 m). The selected study area is covered by 240 pixels by 296 pixels and the corresponding hyperspectral data were classified with an algorithm based on tensor discriminative locality alignment [19]. The obtained land-cover map contains seven classes, namely, shadow, water, road, tree, grass, roof, and trail. The second and third images are two 0.61-m QuickBird images containing 480 pixels by 480 pixels and three multispectral bands, which were acquired in August 2005. One covers the suburb of Xuzhou City, China, whereas the other covers the urban center area of that city. The two images were classified with an algorithm that first integrated spatial features of pixel shape feature set, gray level co-occurrence matrix, and Gabor transform with spectral information and then used a support vector machine for classification. Each generated land-cover map contains seven classes, namely, shadow, water, road, tree, grass, roof, and bare soil. Fig. 2 shows the three images and the classified maps.

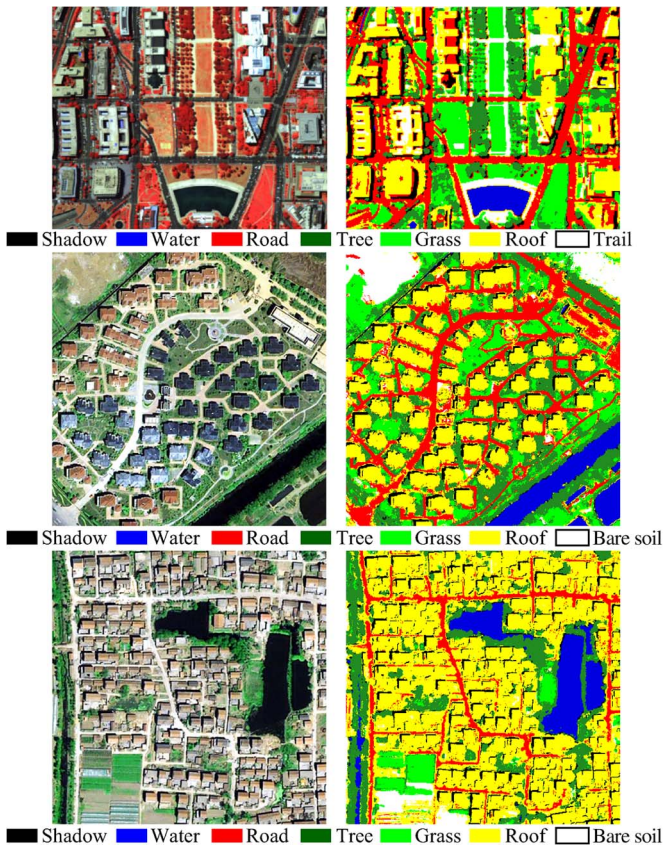

Fig. 2. Three remote sensing images used for testing the proposed AUOC method. (Left) Color images. (Right) Classified land-cover maps used as reference for SPM. (Line 1) Washington, DC map. (Line 2) Xuzhou suburb map. (Line 3) Xuzhou urban center map.

B. Analysis of Local Window Size

The Washington, DC and Xuzhou urban center land-cover maps in Fig. 2 were degraded using three zoom factors, i.e., $S = 3, 5$, and 8, to simulate the coarse proportion images. Using the corresponding three zoom factors, the five STHSPM algorithms (bilinear, bicubic, SPSAM, kriging, and ICK) were then implemented to reproduce the fine spatial resolution maps using the AUOC-based class allocation method. Here, three local window sizes, 3 by 3, 5 by 5, and 7 by 7 (i.e., $N = 3, 5$, and 7), were tested for AUOC. For two maps, the PCC values of the five STHSPM algorithms with different window sizes and zoom factors are shown in Fig. 3. From the bar charts, it is shown that in most cases, the largest PCC was obtained for each STHSPM algorithm when $N = 3$. Guided by the results in Fig. 3, N was set to 3 for the AUOC in the following tests.

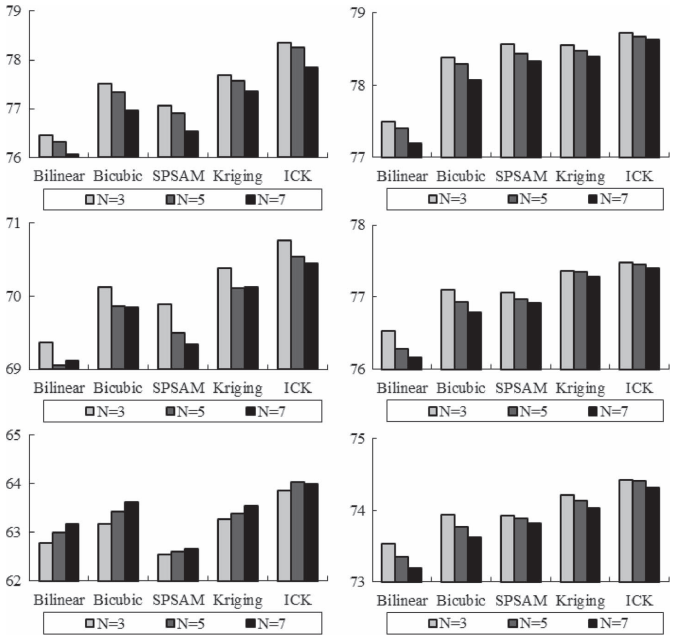

Fig. 3. PCC (in percentage) of the new AUOC method with three local window sizes: $N = 3$, 5, and 7. (Left) Washington, DC map. (Right) Xuzhou urban center map. (Line 1) $S = 3$. (Line 2) $S = 5$. (Line 3) $S = 8$.

C. Results and Analysis

Each reference land-cover map in Fig. 2 was degraded with six zoom factors, i.e., $S = 3, 4, 5, 6, 8$, and 12, to produce six groups of proportion images. The five STHSPM algorithms were then applied, coupled with the UOC- and AUOC-based class allocation methods.

Fig. 4 shows the SPM results of two STHSPM algorithms, i.e., bicubic and SPSAM, using UOC and AUOC for the Washington, DC map with $S = 4$. As shown in the resulting maps, using the AUOC method, the boundaries of classes are smoother and the spatial continuity is greater than for UOC. Focusing on the two marked subareas in the results, we can see clearly that in the UOC results, some pixels for the roof class, which appear as noise or block artifacts, are incorrectly allocated to places that should be the road class. Using the AUOC method, however, this phenomenon is greatly alleviated, and the spatial distribution of the classes is highly similar to that in the reference map. The visual comparison demonstrates that AUOC is capable of obtaining more accurate SPM results than UOC.

For each land-cover map in Fig. 2, the PCC of ten methods (five STHSPM algorithms with two class allocation methods) for each zoom factor S is shown in Fig. 5. From the figure, three observations can be made.

First, consistent with visual inspection, comparison between UOC and AUOC reveals that using the adaptive visiting order of classes, all five STHSPM algorithms produce greater SPM accuracy, particularly for a small zoom factor.

Second, the increase in accuracy from UOC to AUOC is not very obvious for a large zoom factor. More precisely, in the experiments for the three studied images, when S is larger than 6, the difference between AUOC and UOC in terms of PCC is small. This is because both of them are performed based on spatial dependence: They compare the spatial autocorrelation of each class and determine subpixels for class with greater spatial autocorrelation first. When the reference land-cover map

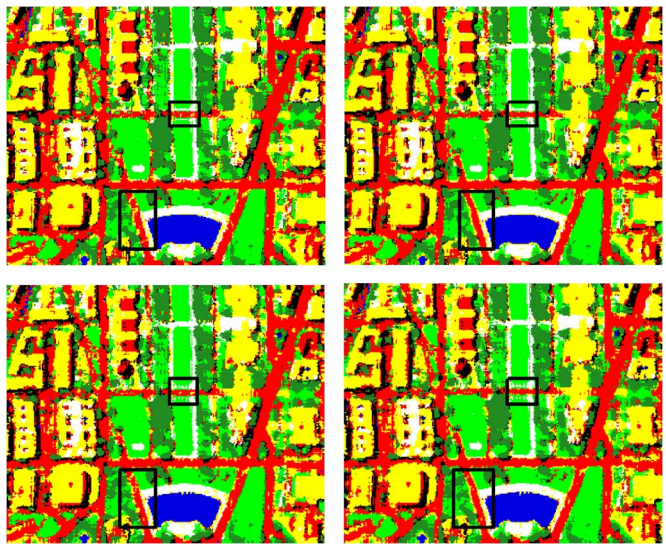

Fig. 4. SPM results of the Washington, DC map ($S = 4$). (Left) UOC. (Right) AUOC. (Line 1) Bicubic results. (Line 2) SPSAM results.

is degraded with large factor S, a number of coarse pixels may be larger than some land-cover objects, which is referred to as the L-resolution case in [1]. In the L-resolution case, however, spatial dependence-based methods usually cannot reproduce objects accurately at a fine spatial resolution. Therefore, the proposed AUOC can enhance UOC when the zoom factor is small, but for large zoom factor, the increase in accuracy may not be very obvious.

Third, the accuracy gain decreases from bilinear to ICK in each row in the figure. The accuracy of STHSPM algorithm is not only related to class allocation but also to soft class value estimation. When the soft class values estimated by the STHSPM algorithms (such as kriging and ICK) are more reliable, the produced SPM result is more accurate, no matter whether UOC or AUOC is used for class allocation. In this case, applying AUOC to such STHSPM algorithms, the room for an increase in accuracy is small.

Table I gives the computing time of UOC and AUOC for the Xuzhou suburb map. We can see that AUOC took more time than UOC. This is because in AUOC, the Moran indices of classes are calculated M times. In UOC, however, the Moran indices are calculated only once. Therefore, AUOC usually requires more computing time than UOC. This is the cost of enhancing SPM accuracy for AUOC. Note that only for small zoom factors, the accuracy improvement merits the extra computational load.

IV. Conclusion

In this letter, a new class allocation method called AUOC has been proposed for STHSPM algorithms. Different from the recently developed UOC method that determines the visiting order of classes based on the global proportion image, the AUOC method uses the local proportion image (i.e., local window) instead. According to the spatial autocorrelation quantified by the Moran index in the local window, AUOC specifies an adaptive visiting order for each coarse resolution pixel and ensures that subpixels for the classes with greater indices are determined first. AUOC inherits the advantages of UOC: It accounts for the intraclass spatial dependence in class allocation

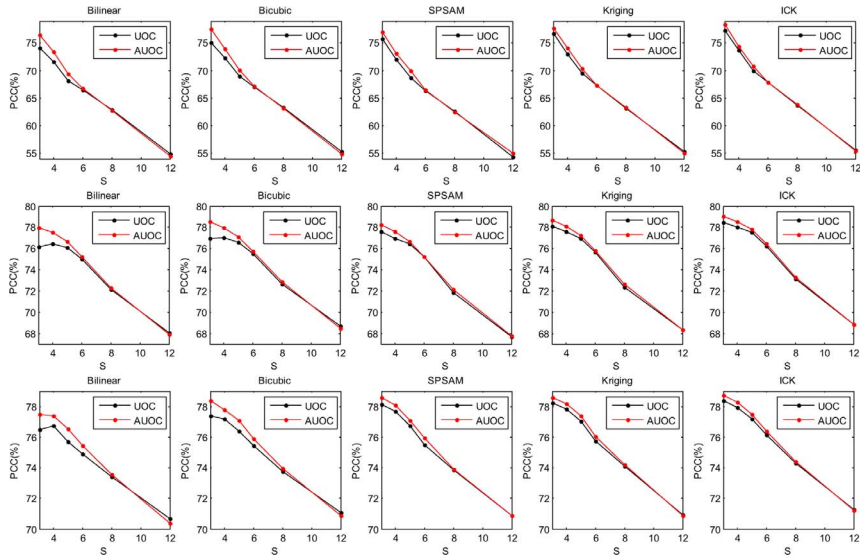

Fig. 5. PCC of five STHSPM algorithms with UOC and AUOC. Line 1: Washington, DC map; Line 2: Xuzhou suburb map; Line 3: Xuzhou urban center map.

TABLE I
COMPUTING TIME (IN SECONDS) OF UOC AND AUOC FOR THE XUZHOU SUBURB MAP

	S=3 (160×160)	S=4 (120×120)	S=5 (96×96)	S=6 (80×80)
UOC	8.4	7.1	6.4	5.7
AUOC	33	19	12	9.1

and does not require prior class information to calculate the Moran index.

In experiments, both UOC and AUOC were applied to five STHSPM algorithms (bilinear, bicubic, SPSAM, kriging, and ICK) and tested on three remote sensing images with multiple zoom factors. Results show that for all five STHSPM algorithms, the proposed AUOC method leads to an increase in accuracy over the existing UOC method for SPM with small zoom factors (e.g., $S < 6$ in this letter). When the zoom factor increases, the advantage of AUOC over UOC in terms of PCC becomes less obvious. Hence, AUOC is recommended as a suitable class allocation method for SPM problems involving a relatively small zoom factor.

ACKNOWLEDGMENT

The authors would like to thank Prof. P. M. Atkinson of the University of Southampton, Southampton, U.K., for his careful proofreading and for helpful suggestions; Dr. L. Zhang of Wuhan University, Wuhan, China, for providing the Washington, DC land-cover map; and the handling editor and anonymous reviewers for their valuable comments.

REFERENCES

[1] P. M. Atkinson, "Issues of uncertainty in super-resolution mapping and their implications for the design of an inter-comparison study," *Int. J. Remote Sens.*, vol. 30, no. 20, pp. 5293–5308, 2009.

[2] Q. Wang, W. Shi, and L. Wang, "Allocating classes for soft-then-hard subpixel mapping algorithms in units of class," *IEEE Trans. Geosci. Remote Sens.*, vol. 52, no. 5, pp. 2940–2959, May 2014.

[3] P. M. Atkinson, "Sub-pixel target mapping from soft-classified, remotely sensed imagery," *Photogramm. Eng. Remote Sens.*, vol. 71, no. 7, pp. 839–846, Jul. 2005.

[4] K. C. Mertens, L. P. C. Verbeke, E. I. Ducheyne, and R. De Wulf, "Using genetic algorithms in sub-pixel mapping," *Int. J. Remote Sens.*, vol. 24, no. 21, pp. 4241–4247, Nov. 2003.

[5] Q. Wang, L. Wang, and D. Liu, "Particle swarm optimization-based sub-pixel mapping for remote-sensing imagery," *Int. J. Remote Sens.*, vol. 33, no. 20, pp. 6480–6496, Oct. 2012.

[6] Z. Mahmood, M. A. Akhter, G. Thoonen, and P. Scheunders, "Contextual subpixel mapping of hyperspectral images making use of a high resolution color image," *IEEE J. Sel. Topics Appl. Earth Observ. Remote Sens.*, vol. 6, no. 2, pp. 779–791, Apr. 2013.

[7] A. M. Muad and G. M. Foody, "Impact of land cover patch size on the accuracy of patch area representation in HNN-based super resolution mapping," *IEEE J. Sel. Topics Appl. Earth Observ. Remote Sens.*, vol. 5, no. 5, pp. 1418–1427, Oct. 2012.

[8] A. J. Tatem, H. G. Lewis, P. M. Atkinson, and M. S. Nixon, "Super-resolution target identification from remotely sensed images using a Hopfield neural network," *IEEE Trans. Geosci. Remote Sens.*, vol. 39, no. 4, pp. 781–796, Apr. 2001.

[9] J. Verhoeye and R. De Wulf, "Land-cover mapping at sub-pixel scales using linear optimization techniques," *Remote Sens. Environ.*, vol. 79, no. 1, pp. 96–104, Jan. 2002.

[10] Q. Wang, W. Shi, and L. Wang, "Indicator cokriging-based subpixel land cover mapping with shifted images," *IEEE J. Sel. Topics Appl. Earth Observ. Remote Sens.*, vol. 7, no. 1, pp. 327–339, Jan. 2014.

[11] H. Jin, G. Mountrakis, and P. Li, "A super-resolution mapping method using local indicator variograms," *Int. J. Remote Sens.*, vol. 33, no. 24, pp. 7747–7773, Dec. 2012.

[12] Y. F. Su, G. M. Foody, A. M. Muad, and K. S. Cheng, "Combining pixel swapping and contouring methods to enhance super-resolution mapping," *IEEE J. Sel. Topics Appl. Earth Observ. Remote Sens.*, vol. 5, no. 5, pp. 1428–1437, Oct. 2012.

[13] V. A. Tolpekin and A. Stein, "Quantification of the effects of land-cover-class spectral separability on the accuracy of Markov-random-field based superresolution mapping," *IEEE Trans. Geosci. Remote Sens.*, vol. 47, no. 9, pp. 3283–3297, Sep. 2009.

[14] F. Ling, Y. Du, F. Xiao, and X. Li, "Subpixel land cover mapping by integrating spectral and spatial information of remotely sensed imagery," *IEEE Geosci. Remote Sens. Lett.*, vol. 9, no. 3, pp. 408–412, May 2012.

[15] X. Li, F. Ling, Y. Du, and Y. Zhang, "Spatially adaptive superresolution land cover mapping with multispectral and panchromatic images," *IEEE Trans. Geosci. Remote Sens.*, vol. 52, no. 5, pp. 2810–2823, May 2014.

[16] F. Ling, Y. Du, X. Li, W. Li, F. Xiao, and Y. Zhang, "Interpolation-based super-resolution land cover mapping," *Remote Sens. Lett.*, vol. 4, no. 7, pp. 629–638, 2013.

[17] Q. Wang and W. Shi, "Utilizing multiple subpixel shifted images in subpixel mapping with image interpolation," *IEEE Geosci. Remote Sens. Lett.*, vol. 11, no. 4, pp. 798–802, Apr. 2014.

[18] X. Xu, Y. Zhong, and L. Zhang, "Adaptive subpixel mapping based on a multi-agent system for remote sensing imagery," *IEEE Trans. Geosci. Remote Sens.*, vol. 52, no. 2, pp. 787–804, Feb. 2014.

[19] L. Zhang, L. Zhang, D. Tao, and X. Huang, "Tensor discriminative locality alignment for hyperspectral image spectral—Spatial feature extraction," *IEEE Trans. Geosci. Remote Sens.*, vol. 51, no. 1, pp. 242–256, Jan. 2013.